Influence of plastic relaxation on the formation of Widmanstätten structures

Maeva Cottura, Benoît Appolaire, Alphonse Finel, Yann Le Bouar

Influence of plastic relaxation on the formation of Widmanstätten structures

Maeva Cottura[1,*], Benoît Appolaire[1], Alphonse Finel[1], Yann Le Bouar[1]

[1]LEM (Onera/CNRS) 29, av. de la Division Leclerc, 92322 Châtillon, France
*Current address: CEA Saclay, DEN/SRMP, 91191 Gif-sur-Yvette, France

Keywords: Diffusive transformation, Widmanstätten, Elasticity, Plasticity

Abstract

A Phase Field model accounting for anisotropic elasticity as well as isotropic strain gradient viscoplasticity is employed to study the growth of acicular precipitates. First, following some recent work [M. Cottura et al., Acta Mater., 2014], it is shown that an anisotropic eigenstrain describing the change in lattice structure during the phase transformation can generate microstructures with the morphological and kinetic feature of Widmanstätten plates. Second, we demonstrate that when isotropic visco-plasticity is accounted for, the plate lengthening remains stationary in isothermal conditions, but features slower growth rates and larger tip radii.

Introduction

Many metallic alloys undergoing allotropic transformations such as steels, brass or Ti-based alloys exhibit colonies of acicular precipitates called Widmanstätten structures resulting from diffusion-controlled phase transformations at high temperatures [1]. Despite different crystallographies, they share generic features: they consist of parallel lamellae that display the same crystalline orientation and, in isothermal conditions, they follow a highly anisotropic stationary growth process. Although extensively studied for many years, it is still unclear how to predict this growth process. We believe that there are two main reasons for this situation. First, because Widmanstätten plates display a constant lengthening rate, models describing dendrite growth during solidification have been applied, which gives the prominent role to the interface energy. If this is legitimate for solid/liquid interfaces, attempts to reproduce Widmanstätten plates with phase field (e.g. [2]) have shown that the required anisotropies of the interface energy feature unrealistic magnitudes. Second, contrary to dendrites, there is no analytical theory encompassing both the diffusion-controlled interface migration and elasticity due to the long range nature of elasticity.
Very recently, we have used the phase field approach to bring new insights into the still debated mechanism selecting the velocity and tip shape by highlighting the prominent role of the elastic driving forces [3]. In particular, we have shown that elastic anisotropy qualitatively changes the growth mechanism that may display a stationary regime. Based on calculations with generic elastic anisotropies, we have succeeded in rationalizing the different occurrences of Widmanstätten structures in different metallic alloys.

Usually, Widmanstätten structures are formed at intermediate temperatures where plasticity may operate to relax the transformation induced stresses. This argument has often been put forward to discard the necessity to involve elasticity in the modeling of diffusion-controlled transformations, contrary to our recent findings (see also [4]). Thus, it is legitimate to question the validity of our previous results when plasticity is accounted for. In this paper, we will address this concern as follows. First, we will present a recent coupling between phase field and isotropic strain gradient plasticity [5]. Then, we will analyze the impact of plasticity on the free growth of acicular precipitates in presence of elastic interactions favoring a single growth direction.

Coupled Model

Phase Field Model

In this work, the Phase Field method has been used for its capacity to handle easily morphological evolutions at the mesoscale and its ability to couple many phenomena. In addition to the local concentration field c($\underline{\boldsymbol{r}}$,t), the model relies on the introduction of a phase field $\varphi(\underline{\boldsymbol{r}}, t)$ displaying constant values in the bulk phases: $\varphi = 0$ in β; $\varphi = 1$ in α. Classically, the mesoscopic free energy functional F is split into chemical, interfacial and elastic contributions. As usually done in mesoscale viscoplastic model, the free energy functional may also contain a viscoplastic contribution F_{vp}. Hence,

$$F = F_{ch}(c,\varphi) + F_{el}(c,\underset{\sim}{\boldsymbol{\varepsilon}}^{el}) + F_{vp}(\underset{\sim}{\boldsymbol{\alpha}}, p) \tag{1}$$

where $\underset{\sim}{\boldsymbol{\varepsilon}}^{el}$ is the elastic strain tensor. F_{vp} as well as the new fields necessary to describe hardening ($\underset{\sim}{\boldsymbol{\alpha}}$, p) will be described hereafter. The chemical free energy F_{ch} accounts for the volume free energy associated with phase transformation and interface energies.

$$F_{ch}(c,\varphi) = \int_V f_{hom}(c,\varphi) + \frac{\lambda_1}{2}|\nabla c|^2 + \frac{\lambda_2}{2}|\nabla\varphi|^2 \; dV \tag{2}$$

where the homogeneous contribution is approximated by a polynomial expansion, whose coefficients are chosen to reproduce the equilibrium concentrations of the coexisting phases [5]. In the framework of linear elasticity, the potential elastic energy reads:

$$F_{el}(\underset{\sim}{\boldsymbol{\varepsilon}}^{el}) = F^a_{el}(\bar{\underset{\sim}{\boldsymbol{\varepsilon}}}) + \frac{1}{2}\int_V \underset{\approx}{\boldsymbol{\lambda}} : \underset{\sim}{\boldsymbol{\varepsilon}}^{el} : \underset{\sim}{\boldsymbol{\varepsilon}}^{el} \; dV \tag{3}$$

where $\underset{\approx}{\boldsymbol{\lambda}}$ is the local elastic tensor and $\bar{\underset{\sim}{\boldsymbol{\varepsilon}}}$ is the average value of the total strain tensor $\underset{\sim}{\boldsymbol{\varepsilon}}(\underline{\boldsymbol{r}})$. $F^a_{el}(\bar{\underset{\sim}{\boldsymbol{\varepsilon}}})$ is an homogeneous term which depends on the choice of the driving conditions. In the present work where stress free conditions have been considered $F^a_{el} = 0$. Assuming that the local concentration is the relevant field for discriminating the elastic properties, $\underset{\approx}{\boldsymbol{\lambda}}$ is assumed to depend linearly on c($\underline{\boldsymbol{r}}$) and is thus space dependent [6]. In the small deformation framework, $\underset{\sim}{\boldsymbol{\varepsilon}}(\underline{\boldsymbol{r}})$ can be divided into three contributions:

$$\underset{\sim}{\boldsymbol{\varepsilon}}(\underline{\boldsymbol{r}}) = \underset{\sim}{\boldsymbol{\varepsilon}}^{el}(\underline{\boldsymbol{r}}) + \underset{\sim}{\boldsymbol{\varepsilon}}^{0}(\underline{\boldsymbol{r}}) + \underset{\sim}{\boldsymbol{\varepsilon}}^{p}(\underline{\boldsymbol{r}}). \tag{4}$$

where $\underset{\sim}{\varepsilon}^0(\underline{\boldsymbol{r}})$ and $\underset{\sim}{\varepsilon}^p(\underline{\boldsymbol{r}})$ are the eigenstrain and plastic strain fields, respectively. Assuming Vegard's law, $\underset{\sim}{\varepsilon}^0(\underline{\boldsymbol{r}}) = \underset{\sim}{\varepsilon}^T \Delta c(\underline{\boldsymbol{r}})$ where $\underset{\sim}{\varepsilon}^T$ stands for the eigenstrain associated with the precipitate of α phase. In diffusive phase transformations, static mechanical equilibrium can be assumed because the relaxation of the elastic waves is by orders of magnitude faster than the evolution of c and φ. In the case of homogeneous elasticity, this problem can be solved analytically in Fourier space [7]. Otherwise, a fixed-point algorithm is used at each time step to numerically solve mechanical equilibrium [6].

The concentration and order parameter evolution is governed by kinetic equations relating time derivatives to the corresponding driving forces, defined as the functional derivatives of F with respect to the fields (noted $\delta F/\delta.$). Assuming linear constitutive relationships, the Cahn-Hilliard equation is derived for the conserved concentration field and the Allen-Cahn equation for the non-conserved order parameter one:

$$\frac{\partial c}{\partial t}(\underline{\boldsymbol{r}}, t) = M\nabla^2 \frac{\delta F}{\delta c(\underline{\boldsymbol{r}}, t)} \tag{5}$$

$$\frac{\partial \varphi}{\partial t}(\underline{\boldsymbol{r}}, t) = -L \frac{\delta F}{\delta \varphi(\underline{\boldsymbol{r}}, t)} \tag{6}$$

M and L are assumed constant for simplicity.

Strain gradient Mesoscale Plasticity Model

Following [5], the Phase Field method is coupled to a mesoscale strain gradient viscoplastic model, similar to the one proposed in [8] which has the advantage of being simple and in which the intrinsic plastic length is easily controlled through the value of a single parameter. Also, for the sake of simplicity, the present formulation is limited to isotropic viscoplasticity even though the extension to an anisotropic viscoplastic behavior could be obtained by explicitly introducing an appropriate set of slip systems. The full model derivation within a coherent thermodynamic framework is presented in [5].

The free energy depends on two viscoplastic internal variables $\underset{\sim}{\boldsymbol{\alpha}}$ and p related to kinematic and isotropic hardening, respectively [9], as follow:

$$F_{vp}(\underset{\sim}{\boldsymbol{\alpha}}, p) = \int_V \frac{1}{3} C\, \underset{\sim}{\boldsymbol{\alpha}} : \underset{\sim}{\boldsymbol{\alpha}} + \frac{1}{2} H\, p^2 + \frac{1}{2} A\, |\nabla p|^2\, dV \tag{7}$$

The last term in (7), proportional to the square gradient of p introduces an intrinsic length scale in the plastic model $\tilde{\xi} = \sqrt{A/E}$ defined in [5], E being Young's modulus. The thermodynamic forces associated with the internal variables are given by:

$$\underset{\sim}{\boldsymbol{X}} = \frac{\delta F}{\delta \underset{\sim}{\boldsymbol{\alpha}}} = \frac{2}{3} C\, \underset{\sim}{\boldsymbol{\alpha}} \tag{8}$$

$$R = \frac{\delta F}{\delta p} = H\, p - A\, \Delta p \tag{9}$$

These thermodynamic forces correspond to the hardening variable defining the elastic domain and the corresponding plastic/viscoplastic potential [9]. More precisely, $\underset{\sim}{\boldsymbol{X}}$ is the center of the elastic domain, and R is its radius.

The kinetic equations of the viscoplastic model are expressed as:

$$\dot{p} = \left\langle \frac{J_2(\underset{\sim}{\boldsymbol{\sigma}} - \underset{\sim}{\boldsymbol{X}}) - R_0 - R}{K} \right\rangle^N \tag{10}$$

$$\underset{\sim}{\dot{\boldsymbol{\varepsilon}}}^p = \frac{3}{2}\,\dot{p}\,\frac{\underset{\sim}{\boldsymbol{\sigma}}' - \underset{\sim}{\boldsymbol{X}}'}{J_2(\underset{\sim}{\boldsymbol{\sigma}} - \underset{\sim}{\boldsymbol{X}})} \tag{11}$$

$$\underset{\sim}{\dot{\boldsymbol{\alpha}}} = \underset{\sim}{\dot{\boldsymbol{\varepsilon}}}^p - D_p\,\underset{\sim}{\boldsymbol{\alpha}}\,\dot{p} \tag{12}$$

$\dot{p}$ follows a Norton type flow rule with $J_2(\underset{\sim}{\boldsymbol{S}})$ the second invariant of the deviatoric stress $\underset{\sim}{\boldsymbol{S}}$, and where R_0 is the initial yield stress and R the isotropic hardening. It is worth noting that R includes both linear isotropic hardening and the strengthening resulting from the plastic size effect (9).

In heterogeneous materials, the viscoplastic parameters C, D_p, A, N, K and R_0 depend on the position $\underline{\boldsymbol{r}}$. In our case, only β undergoes plastic strain while α behaves elastically. To reproduce this behavior all the viscoplastic parameters have been set at their value in the β phase, except the initial yield stress R_0 which is interpolated as follows $R_0(\underline{\boldsymbol{r}}) = \bar{R}_0 + R_0' \tanh\left[\theta\,(\varphi^2(\underline{\boldsymbol{r}}) - 1/2)\right]$ with $\bar{R}_0 = (R_0^\alpha + R_0^\beta)/2$, $R_0' = (R_0^\alpha - R_0^\beta)/2$ and θ a parameter controlling plasticity in the interface.

Model parameters

σ_{int} (mJ.m^{-2})	D (m^2.s^{-1})	C_{11} (GPa)	C_{12} (GPa)	C_{44} (GPa)	C (GPa)	D_p	N	K (MPa.s$^{1/N}$)
5	$3\ 10^{-19}$	197	144	90	150	1900	5	150

Table 1: Physical quantities used in the Phase Field simulations.

The following calculations are not intended to study a specific material but rather to investigate the generic role of isotropic plasticity during the growth of acicular precipitates in metallic alloys at high temperatures. Consequently, the physical parameters used for the calculations (Tab. 1) are not those of a particular alloy, but have nonetheless been selected to comply with realistic orders of magnitude. Homogeneous elasticity is assumed. The non-dimensional gradient coefficients $\tilde{\lambda}_1 = \lambda_1/(\Delta f d^2)$ and $\tilde{\lambda}_2 = \lambda_2/(\Delta f d^2)$, where d is the grid spacing and Δf is an energy density scale, are chosen as $\tilde{\lambda}_1 = 0.21$ and $\tilde{\lambda}_2 = 9.8\ 10^{-4}$. Without loss of generality, the equilibrium concentrations of the phases are set to $c_\beta^0 = 0$ and $c_\alpha^0 = 1$. We have used $L = 100\ M\ d^{-2}$, where d is the grid spacing, to ensure that kinetics is much faster for φ than for c. M is such as to recover the interdiffusion coefficient D. We have used $\theta = 100$ which leads to variations of the viscoplastic parameters over the grid spacing d, a distance smaller than the interface width. Finally, for purely numerical reasons, the value of R_0^α is chosen large enough (100 GPa) to prevent any plastic relaxation of α even in presence of a characteristic plastic length, and the linear isotropic hardening modulus H and yield stress in β R_0^β are set to zero to mimick a high temperature situation where plastic relaxation always occurs.

Results

Elastic reference case

For the sake of comparison, we first discuss the main features found recently in [3] concerning the basic role played by the anisotropic elasticity in the growth of Widmanstätten plates. We focus here on a particular eigenstrain (only $\varepsilon_{22}^T \neq 0$) which features a single soft elastic direction corresponding to an infinite plate with an interface along [100] as the equilibrium shape. We refer the reader to [3] for a complete investigation of different generic shapes of the eigenstrain able to generate Widmanstätten structures.

Consistently with many experimental observations, we have considered a 2D system with 3D elasticity (invariant along [001]). Preliminary calculations have shown that a 1024×384 nodes box is necessary to consider free growth with the periodic conditions. We have considered a grid spacing $d = 1.8$ nm leading to a total size 1.9×0.7 μm^2. Initially a cylindrical nucleus of radius 9 nm, with a concentration $c_\alpha^0 = 1$ and an eigenstrain $\varepsilon_{22} = 4\%$ is introduced in a supersaturated β matrix with $c_\infty = 0.3$. The initial size has been chosen to be greater than the critical size above which the plate shape induced by the anisotropic elastic energy is favored over the circular shape favored by the isotropic interface energy. Growth is thus promoted along the [100] direction from the very beginning of the process.
The evolution of the tip position, along the horizontal axis, has been determined from the level set $\varphi = 0.5$ (Fig. 1). After a transient stage shorter than 1 min, the growth features a linear lengthening regime. The growth rate is quantitatively measured using a polynomial $ax^n + b$ that fits the position curve after the transient stage (dashed red curve). A linear regime is admitted when $n = 1 \pm 0.01$ for a growth of at least 100 nm. The stationary growth rate is 0.9 nm.s^{-1}. The determination of the tip radius R_p is more involved and relies on high orders interpolations of the phase field to reach a precision smaller than the grid spacing [3]. The evolution of R_p in Fig. 1 starts with a decrease

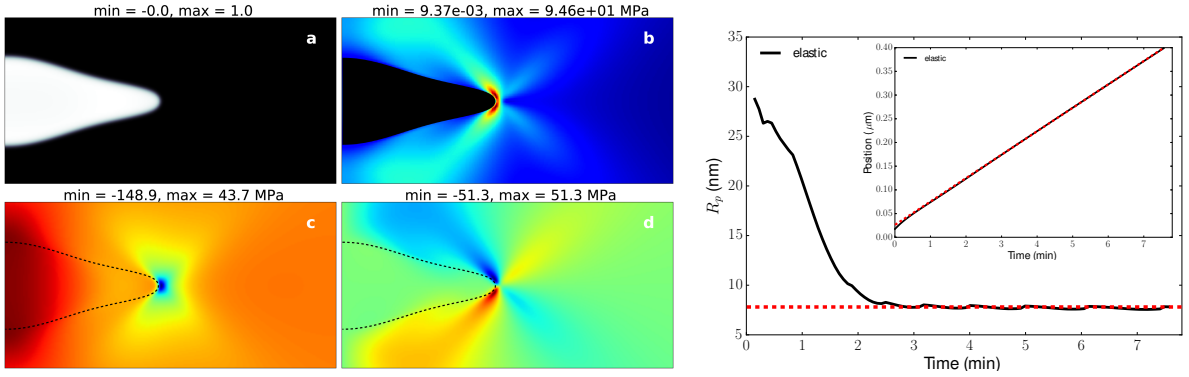

Figure 1: On the left, snaphots (enlargements showing 1/4 and 1/3 of the simulation box along [100] and [010] directions respectively) at $t = 4$ min of a) $\varphi(\underline{\boldsymbol{r}})$ (black: matrix, white: precipitate). b) Effective Von Mises equivalent stress $J_2(\underset{\sim}{\boldsymbol{\sigma}} - \underset{\sim}{\boldsymbol{X}})$ in the matrix. c) $\sigma_{22}(\underline{\boldsymbol{r}})$. d) $\sigma_{12}(\underline{\boldsymbol{r}})$. The color scales are from dark blue to red. On the right, radius of curvature (dashed red curve: average value calculated during the last 4 min) and growth rate (inset) vs. time.

during the first 3 min down to a plateau at the value of 8 nm.

In the snapshots c and d in Fig. 1, we have plotted the distributions of components σ_{22} and σ_{12} respectively: as expected, strong stress concentrations are localized ahead of the plate tip due to its high curvature. σ_{22} is in compression in front of the precipitate and in tension and in tension everywhere else. σ_{12} is non-zero only in front the precipitate exhibiting both tension and compression states, and displays a space distribution quite similar to the one generated by a dislocation. The effective equivalent von Mises stress, i.e. $J_2(\underset{\sim}{\boldsymbol{\sigma}} - \underset{\sim}{\boldsymbol{X}})$, is plotted in Fig. 1b so as to give clues about where plastic relaxation is likely to occur, as discussed in the next section: clearly, plasticity relaxation will be activated in front of the plate tips.

Growth with plastic relaxation

Next, we have investigated the role that viscoplasticity can play in the growth of Widmanstätten plates using the coupled phase field-viscoplasticity model. Beyond the elastic anisotropy that has been shown above to be of prime importance for generating Widmanstätten structures, it is worth emphasizing that ingredients relevant for the present problem are included in the plasticity model such as the hardening and viscosity. In particular, it accounts for the size effect of the plastic behavior beyond the volume fraction effect, i.e. for the hardening (resp. softening) induced by the decrease (resp. increase) of the size of the plastic regions. During the acicular precipitate growth, since the stresses generated by the eigenstrain are strongly localized in front of the precipitate tip as shown above, it is important to account for this size effect.

Considering the same configuration as for the elastic case, we have performed calculations with different values of the intrinsic plastic length $\tilde{\xi}$. Figure 3 compares the corresponding microstructures predicted after $t = 5$ min In all the cases, the initial ellipsoidal precipitates grow from the supersaturated matrix into acicular precipitates elongated along the [100] direction. They all follow stationary growth regimes after short initial transient stages as shown in Fig. 2 (left). Concomitantly, the tip radii R_p decrease during the transient stages down to stationary values (Fig. 2 right). The viscoplastic curves with $\tilde{\xi} = 0$ (red) feature the slowest growth rate with the largest tip radius whereas the elastic

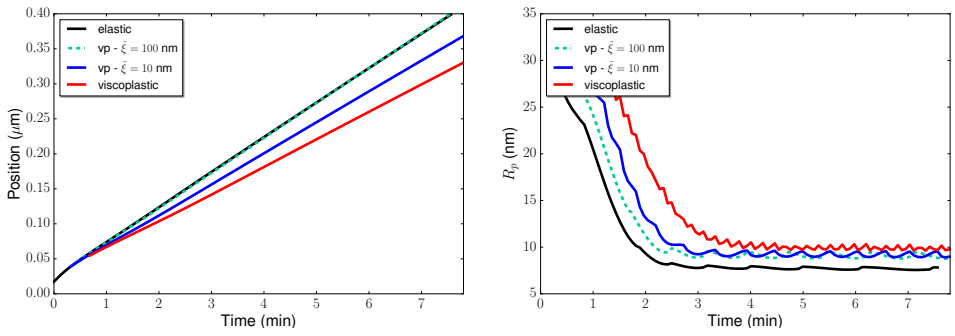

Figure 2: Lengthening (left) and tip radius (right) vs. time for different behaviors of the matrix: elastic and viscoplasticity with different plastic lengths $\tilde{\xi}$.

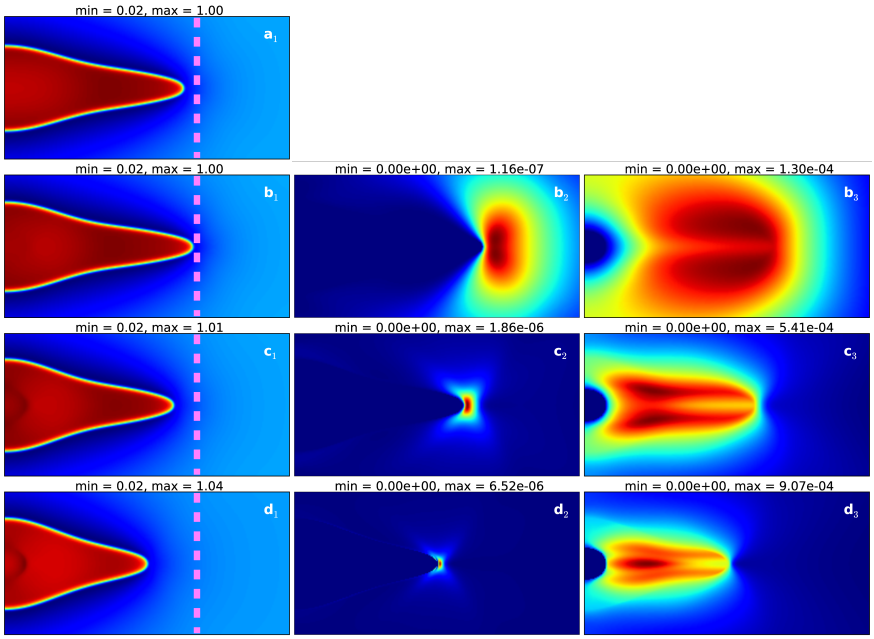

Figure 3: Snapshots (enlargements showing 1/4 and 1/3 of the simulation box along [100] and [010] directions respectively) at $t = 5$ min of left: $c(\underline{\boldsymbol{r}})$ (blue: matrix, red: precipitate); middle: cumulative plastic strain rate $\dot{p}(\underline{\boldsymbol{r}})$; right: cumulative plastic strain $p(\underline{\boldsymbol{r}})$. a) Elasticity; viscoplasticity with b) $\tilde{\xi} = 100$ nm; c) $\tilde{\xi} = 10$ nm; d) $\tilde{\xi} = 0$. Color scales are from dark blue to red.

ones (black) exhibit the fastest kinetics and the sharpest tip. The cases with $\tilde{\xi} \neq 0$ are in between those limit cases. Hence, plasticity seems to only reduce the growth rate and to coarsen the plate tip without changing the mechanism. It is worth stressing that the case with no contribution from the mechanics cannot be considered as a limit case of plastic relaxation, as usually implicitly assumed in the modeling of diffusion-controlled transformations. Indeed, neglecting elasticity would simply generate circular precipitates.

In Fig. 3, in agreement with the distribution of the equivalent Von Mises stress in Fig. 1b, the plastic strain is non-zero mainly in front of the plate tip. The distribution of the plastic strain (right column) explains the decrease in growth rate with respect to the elastic case because it relaxes the coherent stresses at the interface near the precipitate tip. The plastic length introduces several differences with conventional plasticity (Fig. 3b-c) (i) plastic activity is weaker; (ii) p varies more smoothly and (iii) p is more diffuse than when $\tilde{\xi} = 0$. The first point can be attributed to the hardening associated with the confinement of plasticity in a region close to the tip in the matrix. Indeed, the magnitude of this strengthening increases with $|\nabla p|^2$ as given by Eq. 7. It is worth noting that increasing $\tilde{\xi}$ makes β behave purely elastically: the evolutions of the tip position and radius become very close to the elastic behavior when $\tilde{\xi} \to 100$ nm (Fig. 2). To proceed further toward quantitative predictions would require the identification of the intrinsic plastic length by comparison with experimental measurements [5].

Conclusion

The present work has illustrated what role can play isotropic strain-gradient plasticity in the growth of Widmanstätten structures in isothermal conditions. The stationary growth obtained when only elasticity is accounted for is still predicted with plastic relaxation: plasticity only modifies slightly the couple tip radius/growth rate. By relaxing the stress levels, the growth is slowed down and the radius of curvature of the precipitate tip increases. A natural extension of this work would be the investigation of the growth of acicular precipitate colonies. Finally, it would be necessary to extend this study to anisotropic plastic relaxation.

References

[1] B. Appolaire, L. Héricher, E. Aeby-Gautier, Modelling of phase transformation kinetics in Ti alloys isothermal treatments, Acta Mat. 53 (2005) 3001–3011.

[2] I. Loginova, J. Ågren, G. Amberg, On the formation of Widmanstätten ferrite in binary Fe-C –phase-field approach, Acta Mat. 52 (2004) 4055–4063.

[3] M. Cottura, B. Appolaire, A. Finel, Y. L. Bouar, Phase field study of acicular growth: Role of elasticity in widmanstätten structure, Acta Mater. 72 (2014) 200–210.

[4] K. Ammar, B. Appolaire, S. Forest, M. Cottura, Y. Le Bouar, A. Finel, Modelling inheritance of plastic deformation during migration of phase boundaries using a phase field method, Meccanica 49 (2014) 2699–2717.

[5] M. Cottura, Y. L. Bouar, A. Finel, B. Appolaire, K. Ammar, S. Forest, A phase field model incorporating strain gradient viscoplasticity: Application to rafting in ni-base superalloys, J. Mech. Phys. Solids 60 (2012) 1243–1256.

[6] G. Boussinot, Y. Le Bouar, A. Finel, Phase-field simulations with inhomogeneous elasticity comparison with an atomic-scale method and application to superalloys, Acta Mat. 58 (2010) 4170–4181.

[7] A. G. Khachaturyan, The Theory of Structural Transformations in Solids, Wiley, New York, 1983.

[8] S. Forest, E. C. Aifantis, Some links between recent gradient thermo-elasto-plasticity theories and the thermomechanics of generalized continua, Int. J. Solids Struct. 47 (2010) 3367–3376.

[9] J. Lemaitre, J.-L. Chaboche, Mechanics of Solid Materials, Cambridge University Press, 1990.